Optimizing anthocyanin Oral delivery : Effects of food biomacromolecule types on Nanocarrier performance for enhanced bioavailability

Food Chemistry

Yuan, Yu; Hu, Yulin; Huang, Jing; Liu, Bin; Li, Xin et al

https://doi.org/10.1016/j.foodchem.2024.139682

Food Chemistry 454 (2024) 139682

Contents lists available at ScienceDirect

Food Chemistry

journal homepage: www.elsevier.com/locate/foodchem

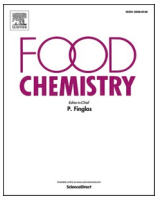

Optimizing anthocyanin Oral delivery: Effects of food biomacromolecule types on Nanocarrier performance for enhanced bioavailability

Yu Yuan [a,1], Yulin Hu [a,1], Jing Huang [a], Bin Liu [a], Xin Li [a], Jinlong Tian [b], Renko de Vries [c], Bin Li [b,*], Yuan Li [a,*]

[a] Research Center of Food Colloids and Delivery of Functionality, College of Food Science and Nutritional Engineering, China Agricultural University, Beijing, 100083, China

[b] College of Food Science, National Engineering and Technology of Research Center for Small Berry, Key Laboratory of Healthy Food Nutrition and Innovative Manufacturing, Liaoning Province, Shenyang Agricultural University, Shenyang, Liaoning 110866, China

[c] Laboratory of Physical Chemistry and Soft Matter, Wageningen University and Research, Stippeneng 4, 6708, WE, Wageningen, the Netherlands

ARTICLE INFO

Keywords:
Food biomacromolecules
Mucus-penetrating
Mucoadhesion
Transmembrane permeability
Bioavailability
Wall materials

ABSTRACT

Wall material types influence the efficacy of nanocarriers in oral delivery systems. We utilized three food biomacromolecules (whey protein isolate, oxidized starch, lipids) to prepare three types of nanocarriers. Our aim was to investigate their performance in digestion, cellular absorption, mucus penetration, intestinal retention, and bioavailability of the encapsulated anthocyanins (Ant). The release rate of protein nanocarriers (Pro-NCs) was twice that of starch nanocarriers (Sta-NCs) and four times that of lipid nanocarriers (Lip-NCs) in simulated gastrointestinal fluid. Additionally, Pro-NCs demonstrated superior transmembrane transport capacity and over three times cellular internalization efficiency than Sta-NCs and Lip-NCs. Sta-NCs exhibited the highest mucus-penetrating capacity, while Pro-NCs displayed the strongest mucoadhesion, resulting in extended gastrointestinal retention time for Pro-NCs. Sta-NCs significantly enhanced the *in vivo* bioavailability of Ant, nearly twice that of free Ant. Our results demonstrate the critical role of wall material types in optimizing nanocarriers for the specific delivery of bioactive compounds.

1. Introduction

Food-derived bioactive compounds, such as anthocyanins (Ant), curcumin, and capsaicin with anti-inflammatory, anti-oxidative, and anti-tumor properties have gained increasing attention for their potential use in preventing diseases like diabetes, cancer, cardiovascular diseases, and obesity(Bao et al., 2021; Dai et al., 2023; Koh et al., 2022). However, their susceptibility to chemical instability in the presence of oxygen, light, low pH, and heat poses a significant challenge(Chai et al., 2018; Chang et al., 2022). The inherent instability of Ant under neutral or alkaline pH conditions, coupled with its limited cellular uptake, strongly restricts absorption in the gastrointestinal tract, resulting in low bioavailability(Shen et al., 2022).

Oral delivery of bioactive compounds faces additional challenges, including rapid metabolism, limited mucus permeability, and low absorption in the intestinal epithelium(Bao et al., 2019). Various delivery systems, such as colloidal capsules(Zhang, Abidi, & Berlin, 2019), solid nanoparticles(Wang, Liu, Liang, Kang, & Wang, 2022), micelles(Jiang et al., 2018), liposome(Wu, Zhang, Li, Secundo, & Mao, 2023), and micro/nano-emulsion(Li et al., 2023), have been proposed to enhance the absorption of bioactive compounds. Nanocarriers play a critical role in protecting and delivering bioactive compounds, improving their stability, solubility, and permeability in the intestinal mucous layer, thus promoting absorption by the intestinal epithelium and ultimately enhancing bioavailability (Yuan et al., 2022).

A growing interest has been observed in the investigation of nano-delivery systems for bioactive compounds, utilizing food biomacromolecules such as proteins, polysaccharides, and lipids. These biomacromolecules are well-known for their non-toxic, biodegradable, and biocompatible nature(Xiong et al., 2020). Moreover, current research on nanocarriers composed of food biomacromolecules focuses extensively on the impact of shape, particle size, and surface charge on the eventual absorption of nanocarriers(Hadji & Bouchemal, 2022). For example, it has been found that mucus permeability of short-sized

* Corresponding authors.
E-mail addresses: libinsyau@163.com (B. Li), yuanli@cau.edu.cn (Y. Li).
[1] Yu Yuan and Yulin Hu contributed equally to this work.

https://doi.org/10.1016/j.foodchem.2024.139682
Received 16 December 2023; Received in revised form 5 April 2024; Accepted 13 May 2024
Available online 16 May 2024

α-lactalbumin nanotubes was superior to that of nanospheres and long-sized nanotubes(Bao et al., 2020). However, different food biomacromolecules, such as proteins, polysaccharides, and lipids, undergo distinct fates in the gastrointestinal tract. Proteins can be digested and hydrolyzed by pepsin in the stomach (Ozel, Zhang, He, & McClements, 2020), lipids are primarily hydrolyzed by pancreatic lipase in the small intestine (Marze, 2022), while polysaccharides like starch, alginate, and pectin can reach the colon due to incomplete digestion in the stomach or small intestine, where they are degraded by gut microbiota (Bello-Perez, Flores-Silva, Agama-Acevedo, & Tovar, 2020; Ling, Wu, Neish, & Champion, 2019; Yuan et al., 2022). Furthermore, the type of the nanocarrier material is also expected to influence their interaction with mucus. Electroneutral or hydrophilic materials with low interaction with mucus layers have demonstrated higher mucus-permeating capacity (Tan et al., 2020), whereas hydrophobic and positively charged materials exhibit strong mucoadhesive properties due to hydrophobic and electrostatic interactions with sialic acid residues of mucins (das Neves, Arzi and Sosnik, 2020; Ubaidulla, Priyanka, Sangavi, & Grace, 2022). In summary, different nanocarrier materials are expected to exhibit distinct physicochemical behavior during the uptake process, strongly influencing the absorption of nanocarriers and, ultimately, the bioavailability of loaded bioactive compounds. However, there has been limited exploration into the comparative effects of different food biomacromolecule types utilized in nanocarrier formulation on bioactive compound delivery, despite the reasonable expectation that it may have a significant impact.

Recognizing the potential substantial impact, we conducted a thorough comparative analysis to acquire a comprehensive knowledge of how the nanocarrier material type influences their uptake, absorption, and, ultimately, bioavailability of the encapsulated bioactive compounds. Specifically, our investigation initially focused on the delivery of a model bioactive compound using various nanocarriers with similar size and shape but varying in the type of food biomacromolecule used in their assembly. Considering whey protein isolate, oxidized starch, stearic acid, and lauric acid as models for protein, starch, and lipid nanocarriers, respectively, we utilized Ant as a model bioactive compound to investigate the loading capacity and *in vitro* release rate of nanocarriers. We compared the cellular uptake and transmembrane transport efficiency of different nanocarriers using an *in-vitro* model of Caco-2 cells. Mucus permeability and biodistribution in the gastrointestinal tract were also compared. Finally, we investigated the intestinal epithelial cell uptake of nanocarriers and the resulting bioavailability of Ant. Through this approach, we aim to achieve a systematic understanding of the impact of nanocarrier material type on various aspects of delivery, including cell endocytosis, biodistribution, and bioavailability.

2. Materials and methods

2.1. Materials

Whey protein isolate (WPI, ≥ 85%), stearic acid (95%), lauric acid (97%), 1,2-distearoyl-*sn*-glycero-3-phosphoethanolamine-N-[methoxy (polyethylene glycol)-5000] (*Mw* = 5000, DSPE-PEG5000), anthocyanins (Ant, cyanidin 3-O-glucoside ≥98%), and soybean lecithin (Mw ≈ 750) were obtained from Sigma-Aldrich (USA). Native soluble potato starch was sourced from AVEBE (Netherlands), and fetal bovine serum (FBS) was acquired from Life Technology (NY, USA). Fluorescent dyes, including rhodamine B, Alexa Fluor™ 488 labeled wheat germ agglutinin (WGA), Phalloidin-FITC, 4′, 6-diamidino-2-phenylindole (DAPI), and the CCK-8 kit were supplied by Fanbo Biochemical (Beijing, China). Minimum Eagle's medium (MEM) and Dulbecco's modified Eagle's medium (DMEM) were bought from Gibco (NY, USA). All chemicals used were high-quality analytical grade. Caco-2 and HT29-MTX (E12) cells were bought from the Cell Resource Center (Peking Union Medical College Headquarters of National Infrastructure of Cell Line Resource, NSTT).

2.2. Preparation of various Nanocarriers

Protein nanocarriers (Pro-NCs) were prepared using a modified thermal crosslinking method(Wu et al., 2015). In detail, a water-in-oil emulsion was formed by mixing soybean oil with 2.5 wt% polyglyceryl polyricinoleate (PGPR) and a 200 mg/mL WPI solution at a volume ratio of 10:1. The mixture was emulsified using an Ultra-turrax T 18 disperser (IKA, Germany) at 13000 rpm for 10 min. Subsequently, the emulsion was heated at 80 °C and centrifuged (13,000 rpm, 20 min) to remove excess oil. Pro-NCs were obtained after washing the precipitate with water three times, followed by freeze-drying and storage at 4 °C for further use.

Starch nanocarriers (Sta-NCs) were prepared through a modified crosslinking method(Li et al., 2020). Firstly, the starch, with a 30% oxidization degree (DO30), underwent modification using a TEMPO-mediated oxidization method(Li et al., 2009). Next, a 50 mg/mL DO30 starch solution was adjusted to pH 10 with 1 M NaOH. Upon adding 250 μL of a 50 mg/mL sodium trimetaphosphate (STMP) solution, this aqueous phase was added into 50 mL n-hexane (oil phase) containing 0.744 g Span 80 and 1.01 g Tween 80. The mixture underwent emulsification for 10 min at a speed of 13,000 rpm, followed by heating at 50 °C for 6 h to facilitate crosslinking. Sta-NCs were obtained by centrifugation (10 min at 12000 rpm) and subsequently washed with ethanol three times. The resulting Sta-NCs were freeze-dried and stored at 4 °C for further use.

Lipid nanocarriers (Lip-NCs) were prepared using a nano-precipitation method referenced to Zhu et al., with slight modifications (Zhu et al., 2017). Specifically, a mixture of stearic and lauric acid (1:4 *w*/w) was dissolved in methanol to achieve a final concentration of 40 mg/mL (fatty acid solution). Lecithin and DSPE-PEG5000 were dissolved in a 4% ethanol aqueous solution to obtain a final concentration of 10 mg/mL with a ratio of 3:1 (*w*/w). The fatty acid solution was then added dropwise into the lecithin solution at a 1:6 volume ratio, followed by emulsification at 3000 rpm for 6 min. The resulting sample was washed three times with water, followed by centrifugation at 13000 rpm (4 °C) for 20 min. Finally, Lip-NCs were freeze-dried and stored at 4 °C for further use.

2.3. Characterization of various Nanocarriers

Dynamic light scattering was employed to characterize the size distribution and ζ-potential of different biomacromolecule nanocarriers at 25 °C. The measurements were conducted using a Nano-ZS 2000 instrument from Malvern Instruments, UK, with a scattering angle of 173° after suitable dilution. Each measurement was performed at least three times. Furthermore, micromorphology images were captured by transmission electron microscopy (TEM) (JEM-1400, JEOL, Japan).

2.4. Loading efficiency of various Nanocarriers

Ant or rhodamine B was incorporated into a 2 mg/mL nanocarrier suspension, stirred for 6 h at 4 °C. To remove free Ant or rhodamine B, ultrafiltration was performed using 3 kD ultrafiltration tubes, and the resulting nanocarriers were washed three times with distilled water. The Ant-loaded nanocarriers or rhodamine B-loaded nanocarriers were then freeze-dried and stored at 4 °C.

To extract the encapsulated Ant or rhodamine B from the freeze-dried samples, acetonitrile was utilized. After 10 min of centrifugation at 13,000 rpm, the supernatant was collected, and the absorbance of Ant at 540 nm and the fluorescence intensity rhodamine B (ex/em = 561/625 nm) were measured by a microplate reader (Infinite M200PRO). The loading efficiency (LE) % was calculated using the following formula:

$$\mathrm{LE\%} = \frac{\mathrm{m(A)}}{\mathrm{m(NCs)} - \mathrm{m(A)}} \times 100\%, \quad (1)$$

where m(A) and m(NCs) represent the amount of Ant in the nanocarriers and nanocarriers (mg), respectively.

2.5. Release behavior of Nanocarriers in stimulated gastrointestinal fluid

To prepare simulated gastric fluid (SGF), a 10 g/L pancreatin aqueous solution was prepared (pH 1.2). For simulated intestinal fluid (SIF), 1 g trypsin was dissolved in a 5 mM KH_2PO_4 buffer with a pH of 6.8. To investigate the release behavior of rhodamine B in SGF, 5 mg/mL various nanocarriers labeled with rhodamine B were dissolved in SGF and then loaded into a dialysis bag with a molecular weight cutoff (MwCO) of 3500 Da (Solarbio, Beijing, China). The dialysis bag containing the nanocarrier solution was immersed in 50 mL of freshly prepared SGF and maintained at 37 °C with gentle stirring for 2 h. At 15 min intervals, a portion of the dialytic SGF was extracted and replaced with an equal volume of fresh SGF. After 2 h, the pH of the dialysis bag solution was adjusted to 6.8 and trypsin was added. The dialysis bag was then immersed in 50 mL of freshly prepared SIF for an additional 6 h. The samples collected were measured by a microplate reader (Bio-Rad, CA, USA). In addition, TEM images of various nanocarriers digested in SGF and SIF were captured.

2.6. Cytotoxicity of various Nanocarriers

Caco-2 cells, obtained from the Beijing Union Medical Cell Resource Center, were cultured in MEM medium supplemented with 10% fetal bovine serum (FBS), streptomycin (100 U mL^{-1}), and penicillin (100 U mL^{-1}) from Invitrogen (CA, USA). The cells were maintained in an incubator at 37 °C with 5% CO_2 and 95% humidity.

To evaluate the cytotoxicity of various nanocarriers, Caco-2 cells were cultured into 96-well plates for 48 h, followed by incubation with different concentrations of biomacromolecule nanocarrier suspensions for 24 h. Subsequently, the suspensions were replaced with 200 μL CCK8 diluent and incubated for an additional 1 h. The absorbance of the samples was measured using a microplate reader at 450 nm. Each experiment was independently performed 6 times.

2.7. Uptake of various Nanocarriers by Caco-2 cells

The uptake of biomacromolecule nanocarriers by Caco-2 cells was assessed using confocal laser scanning microscope (CLSM). Caco-2 cells were cultured with different nanocarriers labeled with rhodamine B at 100 μg/mL, washed with PBS, and labeled with Phalloidin-FITC for the cytomembrane and DAPI for the nuclei. CLSM images were captured using excitations at 488 nm (Phalloidin-FITC), 405 nm (DAPI), and 561 nm (rhodamine B). The cellular uptake was quantitatively evaluated using flow cytometry (FCM, FC500, Beckman) after incubating cells with 100 μg/mL rhodamine B-labeled nanocarriers for 0.5, 1, 2 4, 6, 12, and 24 h.

2.8. Transmembrane permeability of various Nanocarriers in vitro

Caco-2 cells were seeded onto 12-well Transwell® inserts with a pore size of 0.4 μm, a diameter of 12 mm (Corning), and cultured at 37 °C with 5% CO_2. *trans*-Epithelial electrical resistance (TEER) of the monolayers was measured at indicated time points using an electrical resistance system (Millipore Corporation, USA). After approximately 21 days of culture, TEER values exceeding 600 Ω•cm^2 were selected for further experiments. Subsequently, 5 mL of 100 μg/mL rhodamine B-labeled nanocarriers were added to the apical chamber and incubated for 2 h. 200 μL samples were collected from the basolateral chamber, and their absorbance was measured at 540 nm. Each experiment was independently conducted three times. CLSM was used to observe the transmembrane permeability of different nanocarriers. The apparent permeability coefficient (P_{app}) was calculated using the following formula:

$$P_{app} = (dQ/dt)/(A \times C_0) \quad (2)$$

where dQ/dt is the translocation of rhodamine B-labeled nanocarriers from the apical compartment to the basolateral compartment (μg/s). A is the diffusion area of the monolayers (1.12 cm^2), and C_0 is the initial concentration of the rhodamine B-labeled nanocarriers in the apical compartment (μg/mL).

2.9. Animal care

Male Sprague-Dawley (SD) rats and BALB/c mice were obtained from WTLH Bioscience Co, China. The animals were provided *ad libitum* access to rat chow and tap water. All experimental procedures involving animals were conducted in accordance with the Guide for the Care and Use of Laboratory Animals and approved by the Experimental Animal Ethics Committee in Beijing, and the number of the approved protocols of the laboratory/investigator is AW10304204–5-2.

2.10. Ex vivo mucus permeability

To investigate muco-adhesion and mucus permeability, SD rats were anesthetized by isoflurane inhalation and sacrificed by cervical dislocation, the jejunum of sacrificed male SD rats was excised and cut into small loops after the contents were removed. Following mucus staining with Alexa Fluor™ 488-WGA, rhodamine B-labeled nanocarriers were slowly injected into the jejunum segments. Both ends of the jejunum were ligated, and the segments were incubated in PBS at 37 °C for 30 min before observation by CLSM.

2.11. Retention of Nanocarriers in gastrointestinal tract

The retention behavior of various nanocarriers in the gastrointestinal (GI) tract was investigated by capturing fluorescent images *ex vivo*. After a 12 h fast, BALB/c mice were orally administered rhodamine B-labeled nanocarriers (20 mg/kg). Mice were anesthetized by isoflurane inhalation and sacrificed by cervical dislocation at different time intervals after oral administration, and the GI tract was carefully excised for *ex vivo* imaging (FX Pro, Kodak) at 540 nm excitation and 625 nm emission wavelengths. Image analysis was conducted using Carestream MI SE software.

2.12. Distribution of Nanocarriers in intestinal villi epithelial cells

Ex vivo examination of the transport of various nanocarriers in intestinal villi epithelial cells was investigated. SD rats, fasted for 12 h prior, were intragastrically administered various nanocarriers labeled with rhodamine B. After 2 h, the rats were anesthetized by isoflurane inhalation and sacrificed by cervical dislocation, and the small intestine tissues were carefully dissected, embedded in Tissue-Tek® O.C.T™ Compound, and frozen at −80 °C. Subsequently, 10 μm thick tissue slices were prepared, fixed with 4% paraformaldehyde, and stained sequentially with Alexa Fluor 488-WGA and DAPI to visualize nanocarrier localization. Finally, fluorescent images were captured using CLSM.

2.13. Pharmacokinetic studies

BALB/c mice, fasted for 12 h before pharmacokinetic studies, were orally administered a free Ant solution and three different Ant-loaded nanocarriers, each containing an equal amount of Ant at a dosage of 400 mg/kg body weight (BW). Plasma samples were collected at specific time intervals post-intragastric administration after anesthetized by isoflurane inhalation, centrifuged for 5 min at 7500 rpm to separate the serum. On the last time point, all mice were sacrificed by cervical

dislocation. Ant in serum was extract using a mixture of acetonitrile and ethanol (4:1) containing 1.4% formic acid in double volume. After ultrasonic treatment, the mixture was centrifuged at 12000 rpm for 15 min at 4 °C. The resulting supernatant was then filtered using a 0.22 μm filter membrane and quantified by Ultra Performance Liquid Chromatography (UPLC) with an Agilent ZORB A × SB-C18 column (4.6 mm × 250 mm). The elution solvents consisting of acetonitrile (A) and 1% formic acid solution (B) at the proportion of 10% A and 90% B flowed at a rate of 0.1 mL/min. Prism software (version 6.0) was employed for data analysis to determine pharmacokinetic parameters. The absolute bioavailability (F_{Abs}) was determined by the following equation (Bao et al., 2020):

$$F_{Abs} = \frac{AUC_{oral}}{V_{oral} \times Dose} \quad (3)$$

where AUC_{oral} is the area of Ant plasma concentration and time profile, V_{oral} is the volume of oral administration and Dose is the concentration of Ant.

2.14. Statistical analysis

The results are presented as mean ± standard deviation. Statistical analyses were performed using Student's *t*-test, and a probability value (P) of <0.05 was considered statistically significant (*$P < 0.05$).

3. Results and discussion

3.1. Characterizations of Nanocarriers fabricated from different food macromolecules

To investigate the effect of nanocarrier material type on delivery efficiency, WPI, oxidized starch, and lipids were used to fabricate various nanocarriers. Fig. 1A illustrates the formation of protein nanocarriers (Pro-NCs) by heating WPI, driven by hydrophobic interactions, hydrogen bonds, and disulfide bonds(Chen et al., 2022). For starch nanocarriers (Sta-NCs), TEMPO oxidation improved the water solubility of starch(Wang et al., 2015). Subsequently, cross-linking of oxidized starch with sodium trimetaphosphate (STMP) resulted in the formation of Sta-NCs using an emulsion template method(Bao et al., 2019). Lastly, lipid nanocarriers (Lip-NCs) were prepared from food-derived lauric acid and stearic acid *via* nanoprecipitation and homogenization (Zhu et al., 2017). TEM images depicting the microstructure of the nanocarriers are presented in Fig. 1B. All nanocarriers exhibited a uniform spherical shape with a size range of 80 to 110 nm (Fig. 1C). The average diameter for Pro-NCs, Sta-NCs, and Lip-NCs was 110 nm, 80 nm, and 90

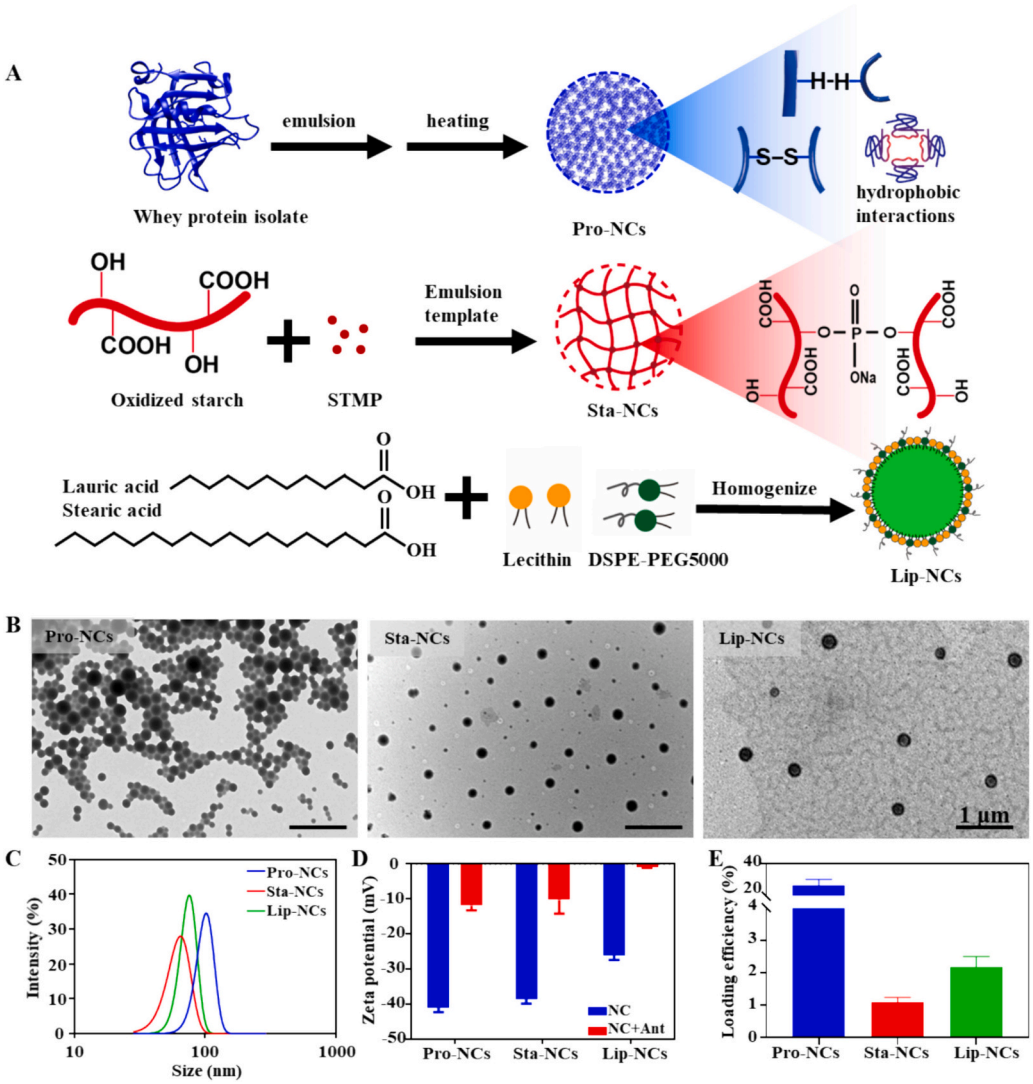

Fig. 1. Characterization of different nanocarriers. (A) Schematic illustration of the construction of Pro-NCs, Sta-NCs, and Lip-NCs. (B) TEM images, (C) size distributions as determined using DLS, and (D) ζ -potential of Pro-NCs, Sta-NCs, and Lip-NCs. (E) Loading efficiency of Ant in Pro-NCs, Sta-NCs, and Lip-NCs. Results are expressed as mean ± SD ($n = 3$).

nm, respectively. Dynamic light scattering experiments revealed that all nanocarriers carried a negative charge in water, with ζ-potentials of −41.07 ± 1.29 mV for Pro-NCs, −38.70 ± 1.25 mV for Sta-NCs, and −26.17 ± 1.26 mV for Lip-NCs (Fig. 1D).

Anthocyanin (Ant) was used as a model bioactive compound to be encapsulated in nanocarriers. The nanocarriers were formed through a heating process, and incorporating Ant post-nanoparticle preparation allowed us to protect its bioactivity. Notably, the ζ-potentials of the nanocarriers decreased after loading Ant, due to the charge neutralization effects (Fig. 1D). This approach was chosen to optimize the preservation of Ant's bioactivity while still benefiting from the advantages of the formed nanocarriers. The loading efficiency of Ant was also investigated, revealing that Pro-NC showed the highest loading efficiency (26.53%) in contrast to Sta-NCs and Lip-NCs (1.09% and 2.19%, respectively). This superior efficiency in Pro-NCs can be attributed, in part, to their high net charge (Fig. 1E). Furthermore, the literature supports our observation that Ant can spontaneously form complexes with WPI primarily through hydrophobic interactions, potentially contributing to the improved loading efficiency of Pro-NCs (Fu et al., 2024). However, the lower oxidization degree of Sta-NCs and the presence of crystalline fatty acids in Lip-NCs may account for their comparatively lower loading efficiency (Wang, Li, Chen, Xin, & Yuan, 2013). For subsequent experiments, nanocarriers with a consistent 1% Ant loading were used to specifically investigate the influence of nanocarrier material on absorption and transportation.

3.2. Release behavior of various Nanocarriers in simulated gastrointestinal fluids

To evaluate the structural transformations of the three types nanocarriers in gastrointestinal fluids, their morphology post-digestion in simulated gastric fluid (SGF) and simulated intestinal fluid (SIF) was examined using TEM (Fig. 2A). During SGF digestion, Pro-NCs exhibited a reduction in size and lower number density, indicative of digestion by pepsin. This suggests that thermal cross-linking did not offer complete protection of Pro-NCs against enzymatic degradation. When transferred into SIF for 2 h, Pro-NCs underwent complete degradation. In the case of Sta-NCs, TEM images suggested a roughened surface in SGF, with nanocarriers appearing fragmented by amylase in SIF. Lip-NCs, on the other hand, remained relatively intact in SGF, with an observed increase in size in both SGF and SIF. We speculate that the composite membrane of Lecithin and DSPE-PEG5000 in Lip-NCs may offer some protection against lipase degradation.

Rhodamine B was loaded into the nanocarriers to investigate release kinetics under simulated gastrointestinal fluids (Fig. S1) due to the instability of Ant at different pH(Ghareaghajlou, Hallaj-Nezhadi, & Ghasempour, 2021). Nanocarriers with a consistent 0.36% loading efficiency of rhodamine B were used for subsequent experiments. Fig. 2B presented additional data illustrating the release behavior of rhodamine B from various nanocarriers in SGF for 2 h and in SIF for an additional 6 h. The release rate of rhodamine B from Pro-NCs was higher than that from Sta-NCs and Lip-NCs in both SGF and SIF. Sta-NCs showed the lowest release rate in SGF, while the release rate in SIF was higher than

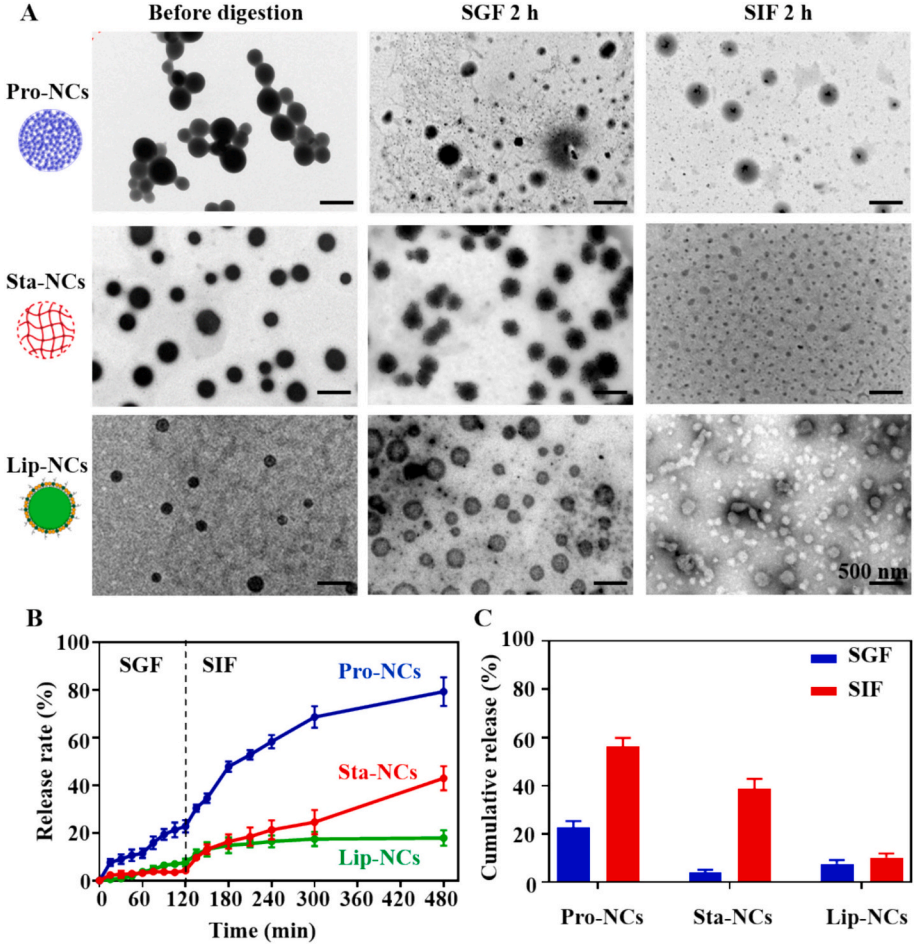

Fig. 2. Simulated digestion of different nanocarriers and impact on bioactive compound release. (A) TEM images of different nanocarriers digested by SGF and SIF at different times. (B) Release kinetics of rhodamine B from different nanocarriers in SGF for 2 h and a further 6 h in SIF (C) Cumulative release of rhodamine B from different nanocarriers in SGF for 2 h and a further 6 h in SIF. Results are expressed as mean ± SD (n = 3).

that of Lip-NCs. Cumulative releases calculated from the release kinetics are shown in Fig. 2C. Pro-NCs exhibited the highest release both in SGF (22.8%) and SIF (56.5%) due to digestion in simulated gastrointestinal fluid, which was in accordance with previous literature(Yuan et al., 2022). Sta-NCs showed minimal rhodamine B release in SGF (4.2%), but a notable release of 38.8% after 6 h of digestion in SIF. This suggests that the increased charge density and larger pore size of Sta-NCs in response to the pH shift may contribute to enhanced release of rhodamine B in SIF. Additionally, the increased salt concentration in SIF may further promote release of rhodamine B(Wang et al., 2013). These results suggest that Sta-NCs hold potential as an intestinal responsive release nanocarrier capable of protecting bioactive molecules in the stomach. Lip-NCs exhibited the lowest cumulative release rate at 17.9%, consistent with previous literature demonstrating their sustained release behavior in the gastrointestinal tract(Gou et al., 2017).

3.3. Caco-2 cellular endocytosis mechanism and transmembrane transport efficiency of various Nanocarriers

Caco-2 cells were used to study the impact of nanocarrier material type on cellular absorption and transport efficiency. Initially, cytotoxicity of the nanocarriers to Caco-2 cells was studied. Pro-NCs and Sta-NCs exhibited good biocompatibility even at relatively high concentrations (1000 μg/mL), whereas Lip-NCs displayed biocompatibility below 200 μg/mL, as shown in Fig. 3A. The relatively lower biocompatibility of Lip-NCs might be due to the addition of the synthetic DSPE-PEG5000, introduced to enhance stability of Lip-NCs (Rydberg, Arteta, Berg, Lindfors, & Sigfridsson, 2016). Subsequently, internalization of the nanocarriers by Caco-2 cells was analyzed by CLSM and FCM. From 1 h to 4 h, the intracellular fluorescent signal (red) for all these three nanocarriers increased, with Pro-NCs exhibiting the strongest red signal compared to Sta-NCs and Lip-NCs (Fig. 3B), indicating superior endocytosis efficiency in Caco-2 cells. The FCM results in Fig. 3C provided

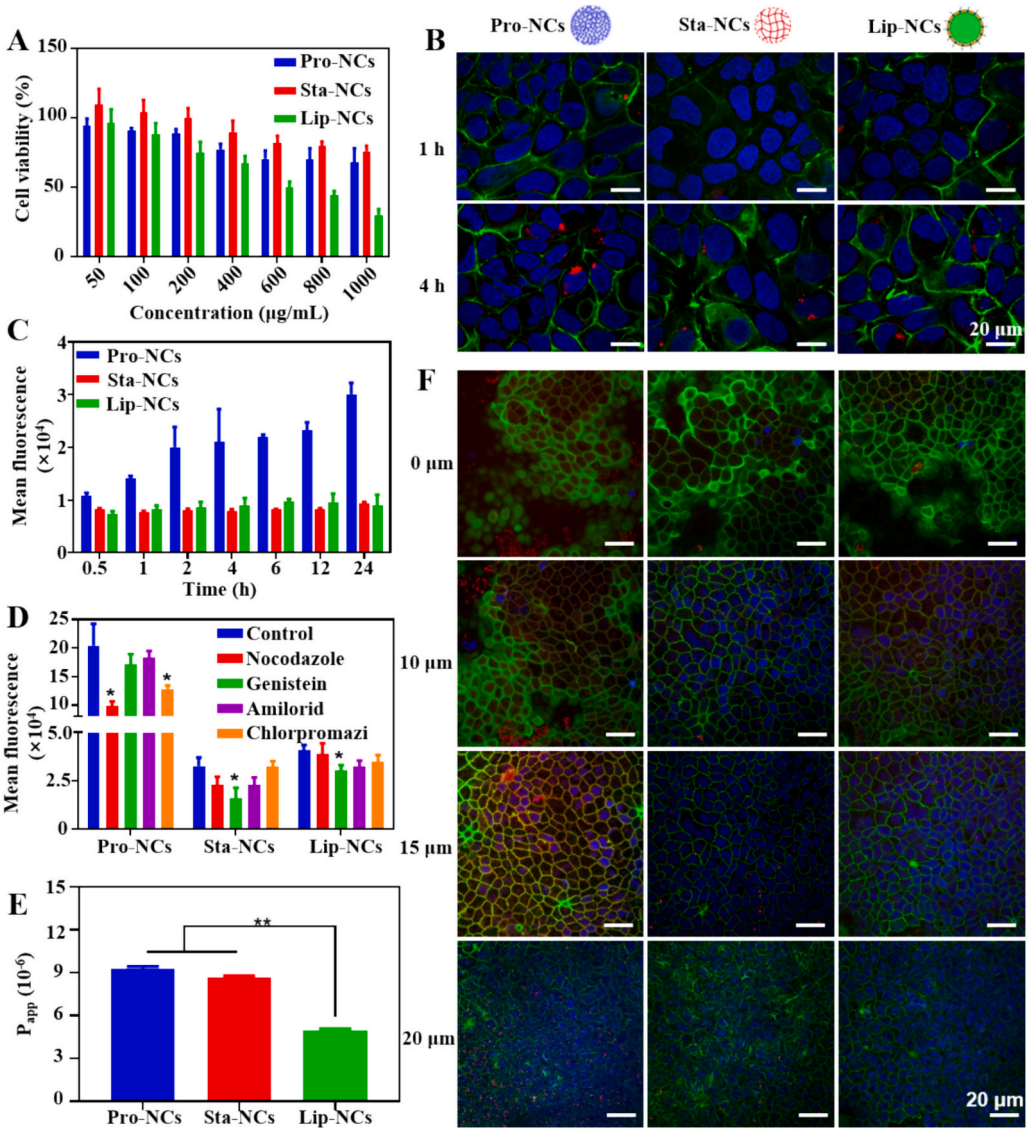

Fig. 3. Cellular uptake of nanocarriers (Pro-NCs, Sta-NCs, and Lip-NCs) in Caco-2 cells. (A) Cytotoxicity of nanocarriers to Caco-2 cells. (B) The images of Caco-2 cells treated with different nanocarriers for 1 h and 4 h. The nuclei, cytomembrane and nanocarriers were stained by DAPI (blue), Phalloidin-FITC (green), and rhodamine B (red), respectively. FCM studies of uptake mechanism of nanocarriers by Caco-2 cells without any inhibitors (C) and in the presence of various inhibitors(D). (E) The apparent transmembrane permeability coefficient P_{app} values indicating the transport of rhodamine B-labeled nanocarriers across Caco-2 cells. (F) The images of Caco-2 cell monolayers cultured with rhodamine B-labeled nanocarriers (red). The nuclei and cytomembrane were stained by DAPI (blue) and Phalloidin-FITC (green), respectively. Results are expressed as mean ± SD ($n = 3$), $^{*}P < 0.05$ *vs* control group, $^{**}P < 0.01$. (For interpretation of the references to colour in this figure legend, the reader is referred to the web version of this article.)

additional confirmation that Pro-NCs exhibited the most pronounced endocytosis across all time points. This observation is consistent with previous findings indicating that protein-stabilized emulsions exhibited higher cellular uptake compared to conventional emulsions (Teo, Lee, Goh, & Wolber, 2017). In contrast, Sta-NCs and Lip-NCs showed a relatively low and constant intracellular fluorescent intensity. The high uptake of Pro-NCs may be due to exposed protein ligands, potentially recognized by membrane receptors, facilitating their cellular internalization(Qiu et al., 2010). Additionally, the lower value of the ζ-potential of Pro-NCs might contribute to improved internalization(Foroozandeh & Aziz, 2018).

The physicochemical properties of nanocarriers may influence not only the degree of uptake, but also the endocytosis mechanism(Li et al., 2023). To investigate this, endocytosis inhibitors including nocodazole, chlorpromazine, genistein, and amiloride, known to inhibit phagocytosis, clathrin-, caveolae-mediated endocytosis, and micropinocytosis, respectively, were used. With high cell viability (>80%) (**Fig. S2**), concentrations of 50 μg/mL nocodazole, and 5 μg/mL of chlorpromazine, genistein, and amiloride were selected for subsequent experiments. In the presence of nocodazole and chlorpromazine, the cellular internalization of Pro-NCs significantly decreased (Fig. 3D), indicating that Pro-NCs were primarily internalized *via* phagocytosis and clathrin-mediated endocytic pathways. This suggests that Pro-NCs might end up in phagolysosomes and lysosomes after endocytosis (Huang, Leshuk, & Gu, 2011). Consistent with literature concerning albumin nanoparticles, our study found that Pro-NCs were primarily internalized through phagolysosomes and the clathrin-mediated pathway (Hillaireau & Couvreur, 2009). In contrast, Sta-NCs and Lip-NCs, as indicated by the impact of genistein treatment, predominantly entered *via* caveolae-mediated endocytosis, potentially escaping lysosome-mediated degradation after endocytosis (Li et al., 2019; Sahay, Alakhova, & Kabanov, 2010). This finding aligns with reports indicating that starch-coated vectors tend to follow the caveolar pathway (Sannidhi et al., 2023). However, Tween 60-stabilized lipid nanocarriers entered *via* both clathrin-mediated and caveolae-mediated endocytosis, potentially attributable to differences in the emulsifier used (Neves, Queiroz, et al., 2016).

Orally administered nanocarriers can only be absorbed after crossing the intestinal epithelial cell layer. Therefore, nanocarriers transport across a Caco-2 cell monolayer was investigated. CSLM images of monolayers without gaps between cells are presented in **Fig. S3**. The apparent transmembrane permeability coefficient (P_{app}) values for permeation from the upper to the lower compartment were quantified. The P_{app} of Pro-NCs (9.29×10^{-6}) was higher than that of Sta-NCs (8.69×10^{-6}) and nearly twice that of Lip-NCs (4.97×10^{-6}), as shown in Fig. 3E. Shen et al. demonstrated a 10.3-fold improvement in the P_{app} of astaxanthin through WPI-stabilized nanodispersions (Shen, Zhao, Lu, & Guo, 2018). Similarly, Wang et al. reported a three-fold increase in the transport of quercetin-loaded carboxymethyl starch microgel across Caco-2 cell monolayers compared to free quercetin (Wang et al., 2024). Additionally, lipid nanoparticles were found to enhance resveratrol permeability by 1.5-fold (Neves, Martins, Segundo, & Reis, 2016). CLSM images of cross-sections through the Caco-2 cell layers in Fig. 3F showed nanocarriers that have penetrated the cell layer to different depths. Fluorescence signals of Pro-NCs were observed from 0 to 20 μm depth after 2 h of incubation, indicating substantial penetration of the cell monolayer. Fluorescence signals were also observed at 15 μm for Sta-NCs, whereas signals for Lip-NCs were nearly undetectable. Therefore, the cellular internalization efficiency of Pro-NCs and Sta-NCs surpassed that of Lip-NCs. Notably, it has been reported that proteins and starch can open tight junctions between epithelial cells, contributing to the transport of nanocarriers across epithelial cell layers(Afzal et al., 2023; Déat-Lainé, Hoffart, Garrait, & Beyssac, 2013).

3.4. Mucus penetration and Mucoadhesion of Nanocarriers

The intestinal mucus layer plays a crucial role in capturing and removing foreign nanocarriers and pathogens through adhesion and steric effects. Hence, nanocarriers can only be efficiently absorbed after penetrating this mucus layer(Subramanian, Langer, & Traverso, 2022). A superior mucus penetration ability allows nanocarriers to rapidly penetrate the intestinal mucus layer, thus promoting absorption. Additionally, adhesion to mucus can also improve the absorption of nanocarriers by prolonging residence time in the intestine. To explore the adhesion and penetration effects of the three types of nanocarriers in intestinal mucus, rhodamine B-labeled Pro-NCs, Sta-NCs, and Lip-NCs were injected into excised rat intestines, and the intestinal mucus surface was observed by CLSM. Fig. 4A illustrates that red fluorescence signals on the mucus surface were the strongest for Pro-NCs and lowest for Sta-NCs, indicating strong mucoadhesion for Pro-NCs and weak mucoadhesion for Sta-NCs. The former may be attributed to the formation of hydrogen bonds and disulfide bridges between WPI and mucin (Hsein, Garrait, Beyssac, & Hoffart, 2015). Fluorescence signals on the mucus surface for Lip-NCs were intermediate in strength, possibly due to the long fatty acid chain of lecithin, which may interact favorably with mucus. Subsequently, the penetration behavior of nanocarriers in mucus was investigated and scanned in 3D by CLSM (Fig. 4B). For a schematic representation of nanocarriers penetration into mucus, refer to Fig. 4C. Sta-NCs exhibited the deepest penetration depth, indicating superior penetration capacity. The relatively smaller size of Sta-NCs may have facilitated mucus penetration, and hydrogen bonds between carboxyls of the oxidized starch and mucin may have prolonged the retention time of Sta-NCs, leading to better penetration in the mucus(Serra, Domenech, & Peppas, 2009). In summary, Pro-NCs exhibited the strongest adhesion to the mucus surface, while Sta-NCs demonstrated the ability to penetrate more deeply into the mucus. Only a few Lip-NCs were detected in the mucus. The robust mucus penetration capacity of Sta-NCs may be beneficial to the rapid absorption of bioactive compounds.

3.5. In vivo biodistribution of Nanocarriers

Subsequently, the intestinal retention and biodistribution of rhodamine B-labeled Pro-NCs, Sta-NCs, and Lip-NCs at different time intervals after gavage was investigated (Fig. 5A). At 0.5 h, Sta-NCs had traveled the furthest in the intestine compared to Pro-NCs and Lip-NCs. By 1 h, the red fluorescence signals of Pro-NCs and Lip-NCs indicated significant transport for these nanocarriers in the intestine. Sta-NCs arrived at the cecum after 2 h, with almost no fluorescence signal observed in the intestine after 8 h, suggesting fast absorption of Sta-NCs. Pro-NCs and Lip-NCs did not reach the cecum until 4 h later. Fluorescence signals of Pro-NCs were observed for up to 8 h, suggesting the longest gastrointestinal retention time, consistent with the strong mucoadhesion of the Pro-NCs (Fig. 4). Additionally, the *in vivo* absorption of Pro-NCs, Sta-NCs, and Lip-NCs on intestinal epithelial cells was further investigated. Fasted SD rats were orally administered rhodamine B-labeled nanocarriers for 2 h, and histological sections of the duodenum, jejunum, and ileum were collected and observed by CLSM (Fig. 5B). Due to its ability to adhere to mucus, the red fluorescence signals of Pro-NCs predominantly appeared in the duodenum and jejunum. Most Sta-NCs signals were present in the jejunum and ileum, with Sta-NCs entering the submucosa of the intestine in the jejunum, indicating excellent mucus penetration and absorption ability of Sta-NCs. In contrast, Lip-NCs exhibited weak fluorescence signals in all segments of the intestine, with slightly stronger signals in the jejunum. As illustrated in Fig. 5C, Pro-NCs were mainly distributed in the upper part of intestine (duodenum and jejunum), while Sta-NCs were directed towards the lower part of the intestine (jejunum and ileum), and only a small number of Lip-NCs were present in the jejunum.

In summary, the building materials of nanocarriers have a profound effect on their adsorption behavior in the GI tract. For Pro-NCs, strong

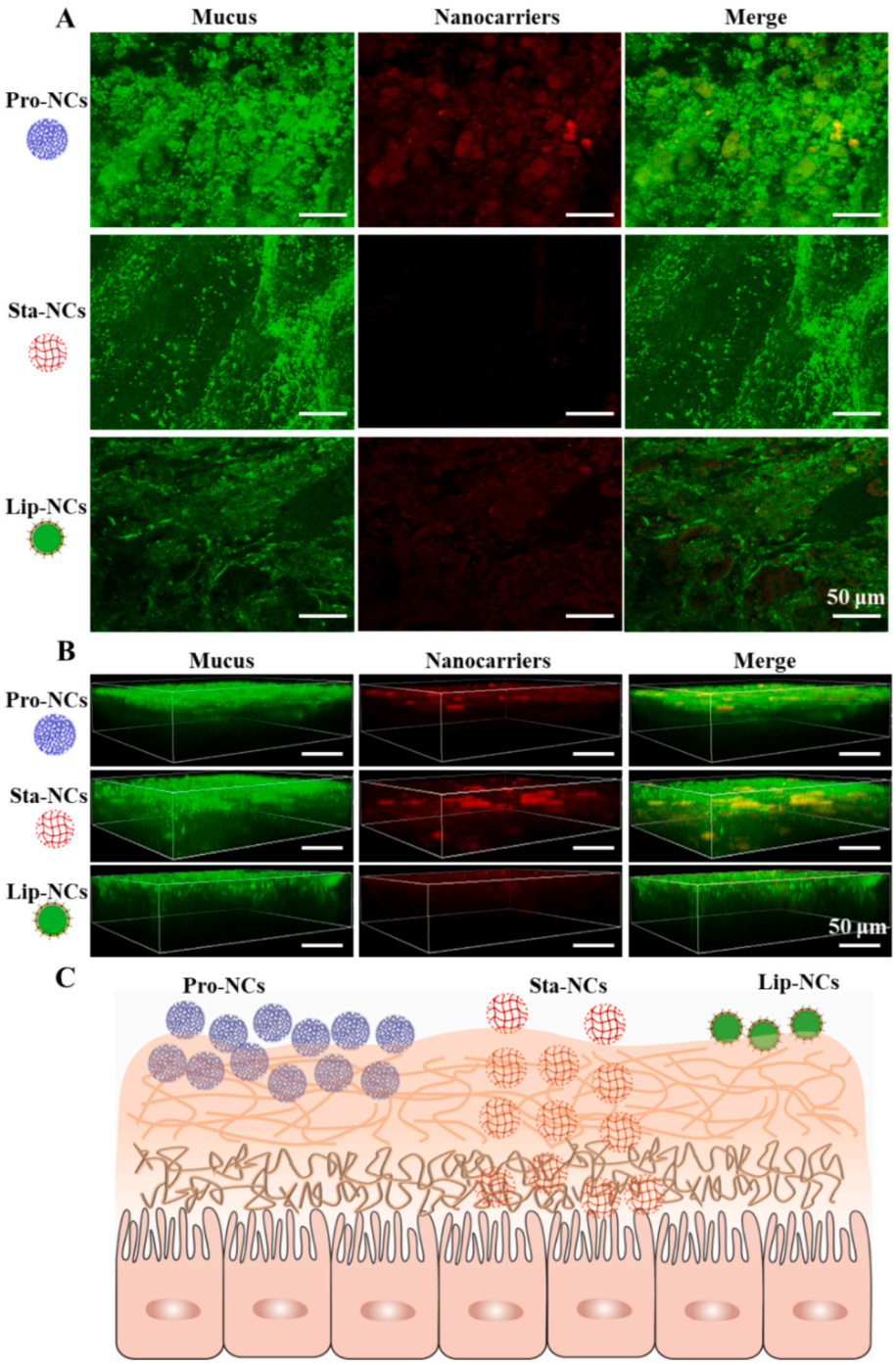

Fig. 4. mucus penetration and mucoadhesion capacity *ex vivo* of different nanocarriers (Pro-NCs, Sta-NCs, and Lip-NCs) (A) 2D images of nanocarriers labeled with rhodamine B (red) adhering to the surface of mucus labeled with Alexa Fluor 488-WGA (green) (B) 3D images of different nanocarriers(red) diffusing in intestinal mucus green) after 0.5 h incubation *ex vivo*. (C) Schematic illustration of mucus penetration of Pro-NCs, Sta-NCs, and Lip-NC. (For interpretation of the references to colour in this figure legend, the reader is referred to the web version of this article.)

mucoadhesion and long retention time promoted absorption, whereas for Sta-NCs, absorption was especially promoted by good penetration into mucus. Finally, Lip-NC lacked both these qualities, presumably leading to lower absorption.

3.6. Bioavailability of anthocyanin-loaded Nanocarriers

The bioavailability of Ant is often limited by its inherent characteristics, such as chemical instability and rapid metabolism(Tong, Li, & Meng, 2023). To evaluate the extent to which different types of nanocarriers can protect Ant and improve its bioavailability, fasted SD rats were orally administered either free Ant or various Ant-loaded nanocarriers, each containing equal amounts of Ant. As shown in Fig. 6A, Ant loaded in Sta-NCs exhibited the highest concentrations at each time point compared to the other two types of nanocarriers, indicating that Sta-NCs significantly improved the bioavailability of Ant. While both Pro-NCs and Lip-NCs enhanced the bioavailability of Ant to varying degrees compared to the group receiving free Ant, their effectiveness was not as pronounced as that of Sta-NCs. Detailed pharmacokinetic parameters, including area-under-the-curve (AUC), peak time

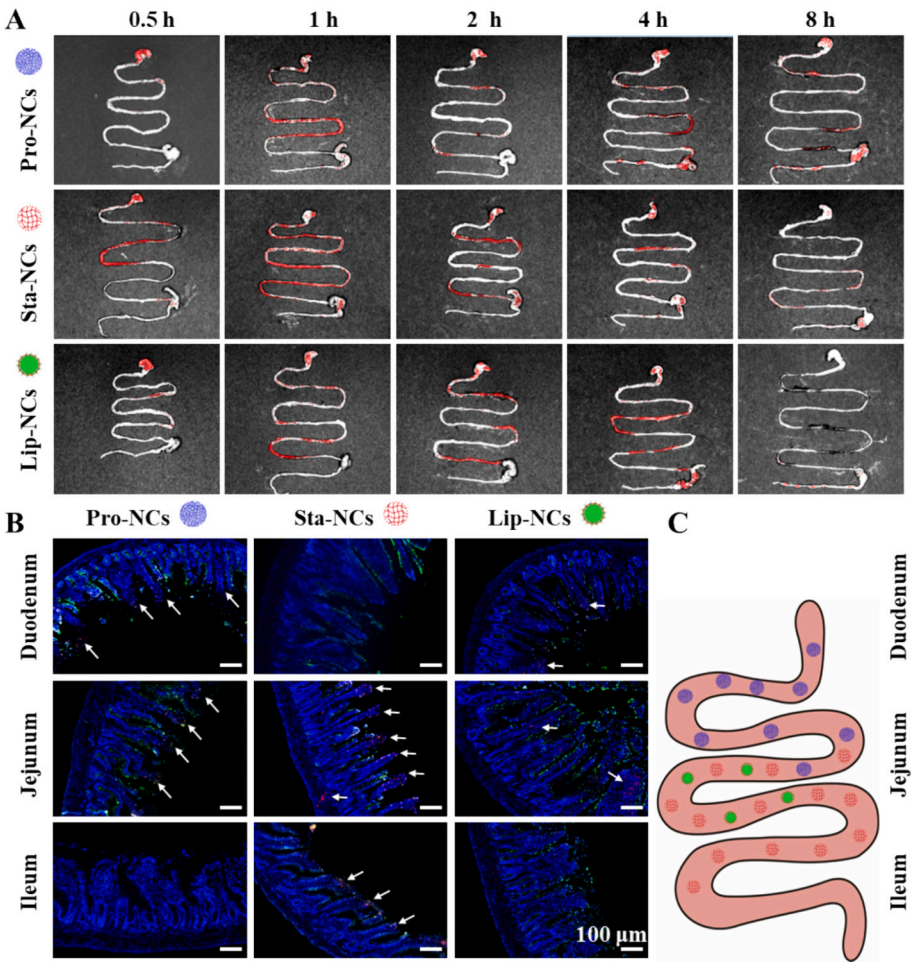

Fig. 5. Biodistribution of different nanocarriers (Pro-NCs, Sta-NCs, and Lip-NCs) in GI tract. (A) *Ex vivo* fluorescence images of nanocarriers labeled with rhodamine B moving through the GI tract as a function of time. (B) Distribution of nanocarriers in intestinal villi epithelial cells after oral administration for 2 h. The nuclei of the villi, mucus, and nanocarriers were labeled by DAPI (blue), Alexa Fluor 488-WGA (green), and rhodamine B (red), respectively. (C) Schematic diagram of nanocarriers distribution in small intestine after oral administration for 2. (For interpretation of the references to colour in this figure legend, the reader is referred to the web version of this article.)

(T_{max}) and maximum blood concentration (C_{max}) are provided in Table 1. The C_{max} for all three Ant-loaded nanocarriers occurred 15 min after administration, while the C_{max} for free Ant appeared after 5 min, suggesting a delayed Ant absorption for all nanocarriers. The Sta-NCs group possessed the highest C_{max} (541.67 ng/mL) compared to Pro-NCs (412.27 ng/mL) and Lip-NCs (336.87 ng/mL), along with the largest AUC, which was twice that of free Ant. The absolute bioavailability F_{Abs} in Fig. 6B indicated that all nanocarriers enhanced the bioavailability of Ant compared to orally administered free Ant, with Sta-NCs demonstrating the most significant improvement. The bioavailability of free Ant was <1%, consistent with a previous report (Chang et al., 2022). In addition, starch nanoparticles were reported to increase the bioavailability of paclitaxel by 5.42 times (Wang et al., 2024), and WPI nanoparticles were found to significantly enhance the oral bioavailability of lycopene (Jiang et al., 2018). Moreover, literature supports the notion that lipid nanoparticles can improve the bioavailability of active substances (Talegaonkar & Bhattacharyya, 2019).

As shown in **Fig. 6**C, our study demonstrates that all three types of nanocarriers could overcome the barriers of the mucus and epithelial cell layers, leading to an enhanced bioavailability of the bioactive payload. However, it is crucial to note that substantial variations exist among the three types of nanocarriers made of various materials across various stages of the transport and uptake process. However, to systematically explore the effects of nanocarrier materials on the oral absorption of active substances, further research should be delved into the loading and delivery mechanisms of various compounds.

4. Conclusion

In summary, Pro-NCs exhibit exceptional mucoadhesive capacity, suggesting prolonged gastrointestinal retention time. Moreover, Pro-NCs demonstrate strong endocytosis through phagocytosis and clathrin-mediated endocytic pathways, coupled with a high transmembrane transport capacity. In contrast, Lip-NCs were internalized primarily *via* caveolae-mediated endocytosis. Lip-NCs remained stable and could sustained release Ant in gastrointestinal tract for long time. However, Lip-NCs display limited mucus adhesion and penetration. On the other hand, Sta-NCs are internalized *via* caveolae-mediated endocytosis, escaping degradation in phagolysosomes and lysosomes. Notably, Sta-NCs demonstrate superior mucus penetration, rapidly entering the submucosa of the intestine. Consequently, the bioavailability of Ant is highest when encapsulated in Sta-NCs. In light of these findings, we suggest that Sta-NCs represent the optimal nanocarrier for the oral delivery of bioactive compounds, offering both strong mucus penetration and high bioavailability.

Data availability.

The data that support the findings of this study are available within the article and its supporting information.

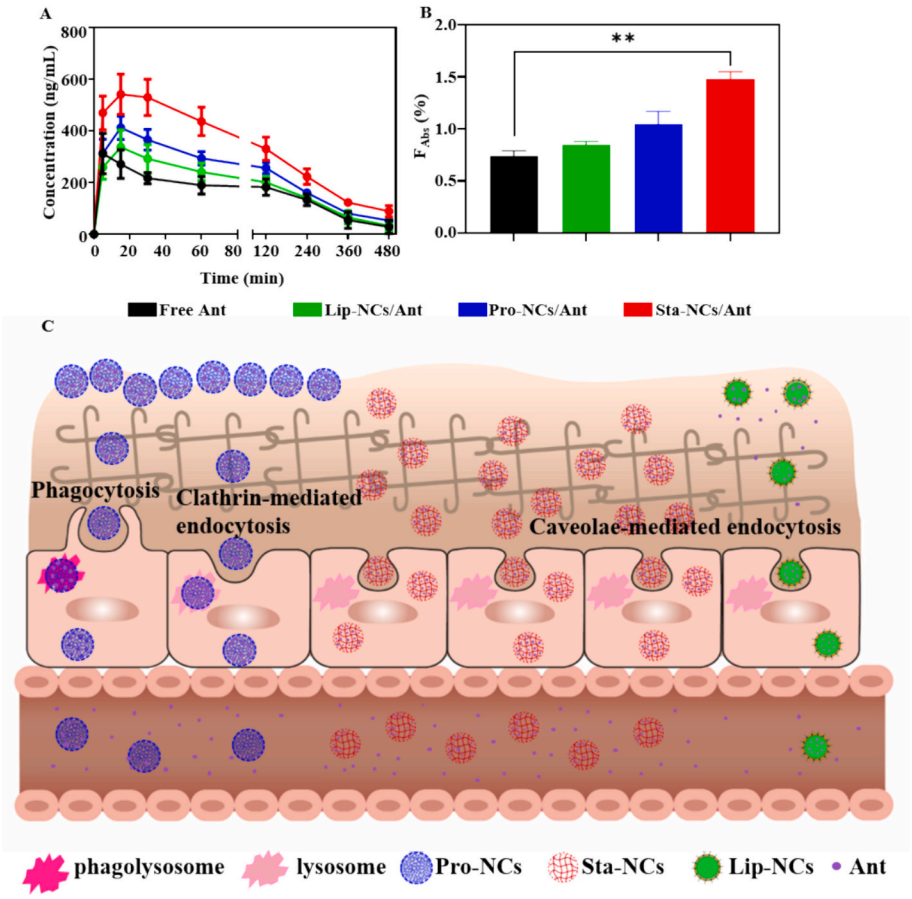

Fig. 6. The bioavailability of Ant. (A) Plasma Ant concentrations at different time points after oral administration of different Ant formulations. (B) the absolute bioavailability (F_{Abs}) of Ant. (C) Schematic illustration of mucus penetration and intracellular pathways of Pro-NCs, Sta-NCs, and Lip-NCs. Data are expressed as mean ± SD ($n = 3$), $^{**}P < 0.01$.

Table 1
Pharmacokinetics parameters of anthocyanin in each treatment group. Data are expressed as mean ± SD (n = 3).

Formulations	C_{max} (ng/mL)	T_{max} (min)	$AUC_{0-\infty}$
Free Ant	312.01 ± 26.63	5	59,765 ± 416
Pro-NCs/Ant	412.27 ± 28.26	15	83,952 ± 950
Sta-NCs/Ant	541.67 ± 20.43	15	118,481 ± 763
Lip-NPs/Ant	336.87 ± 27.77	15	68,218 ± 264

CRediT authorship contribution statement

Yu Yuan: Writing – review & editing, Writing – original draft, Methodology, Investigation. **Yulin Hu:** Writing – review & editing, Writing – original draft, Investigation. **Jing Huang:** Investigation. **Jinlong Tian:** Data curation. **Renko de Vries:** Formal analysis. **Bin Li:** Writing – review & editing, Project administration, Conceptualization. **Yuan Li:** Writing – review & editing, Project administration, Funding acquisition, Conceptualization.

Declaration of Competing Interest

The authors declare that they have no known competing financial interests or personal relationships that could have appeared to influence the work reported in this paper

Data availability

Data will be made available on request.

Acknowledgements

This work was supported by National Natural Science Foundation of China [32172345,
31972202].

Declaration of interests

The authors declare that they have no known competing financial interests or personal relationships that could have appeared to influence the work reported in this paper.

Appendix A. Supplementary data

Supplementary data to this article can be found online at https://doi.org/10.1016/j.foodchem.2024.139682.

References

Afzal, O., Rizwanullah, M., Altamimi, A. S. A., Alossaimi, M. A., Kamal, M., & Ahmad, J. (2023). Harnessing natural polysaccharides-based nanoparticles for oral delivery of phytochemicals: Knocking down the barriers. *Journal of Drug Delivery Science and Technology, 82*. https://doi.org/10.1016/j.jddst.2023.104368

Bao, C., Jiang, P., Chai, J. J., Jiang, Y. M., Li, D., Bao, W. E., & Li, Y. (2019). The delivery of sensitive food bioactive ingredients: Absorption mechanisms, influencing factors, encapsulation techniques and evaluation models. *Food Research International, 120*, 130–140. https://doi.org/10.1016/j.foodres.2019.02.024

Bao, C., Li, Z. K., Liang, S., Hu, Y. L., Wang, X. Y., Fang, B., & Li, Y. (2021). Microneedle patch delivery of capsaicin-containing alpha-Lactalbumin Nanomicelles to adipocytes achieves potent anti-obesity effects. *Advanced Functional Materials, 31* (20), 2011130. https://doi.org/10.1002/adfm.202011130

Bao, C., Liu, B., Li, B., Chai, J. J., Zhang, L. W., Jiao, L. L., & Li, Y. (2020). Enhanced transport of shape and rigidity-tuned alpha-Lactalbumin nanotubes across intestinal mucus and cellular barriers. *Nano Letters, 20*(2), 1352–1361. https://doi.org/10.1021/acs.nanolett.9b04841

Bao, W. E., Liu, X. W., Lv, Y. L., Lu, G. H., Li, F., Zhang, F., & Li, Y. (2019). Nanolongan with multiple on-demand conversions for Ferroptosis-apoptosis combined anticancer therapy. *ACS Nano, 13*(1), 260–273. https://doi.org/10.1021/acsnano.8b05602

Bello-Perez, L. A., Flores-Silva, P. C., Agama-Acevedo, E., & Tovar, J. (2020). Starch digestibility: Past, present, and future. *Journal of the Science of Food and Agriculture, 100*(14), 5009–5016. https://doi.org/10.1002/jsfa.8955

Chai, J. J., Jiang, P., Wang, P. J., Jiang, Y. M., Li, D., Bao, W. E., & Li, Y. (2018). The intelligent delivery systems for bioactive compounds in foods: Physicochemical and physiological conditions, absorption mechanisms, obstacles and responsive strategies. *Trends in Food Science & Technology, 78*, 144–154. https://doi.org/10.1016/j.tifs.2018.06.003

Chang, R. X., Liu, B., Wang, Q. M., Zhang, J. P., Yuan, F., Zhang, H. J., & Li, Y. (2022). The encapsulation of lycopene with α-lactalbumin nanotubes to enhance their antioxidant activity, viscosity and colloidal stability in dairy drink. *Food Hydrocolloids, 131*, Article 107792. https://doi.org/10.1016/j.foodhyd.2022.107792

Chen, S. N., Du, Y. Z., Zhang, H. J., Wang, Q. M., Gong, Y. F., Chang, R. X., & Li, Y. (2022). The lipid digestion behavior of oil-in-water Pickering emulsions stabilized by whey protein microgels of various rigidities. *Food Hydrocolloids, 130*, Article 107735. https://doi.org/10.1016/j.foodhyd.2022.107735

Dai, S. C., Liao, P. L., Wang, Y. L., Tian, T., Tong, X. H., Lyu, B., & Wang, H. (2023). Soy protein isolate-catechin non-covalent and covalent complexes: Focus on structure, aggregation, stability and in vitro digestion characteristics. *Food Hydrocolloids, 135*, Article 108108. https://doi.org/10.1016/j.foodhyd.2022.108108

Déat-Lainé, E., Hoffart, V., Garrait, G., & Beyssac, E. (2013). Whey protein and alginate hydrogel microparticles for insulin intestinal absorption: Evaluation of permeability enhancement properties on Caco-2 cells. *International Journal of Pharmaceutics, 453*(2), 336–342. https://doi.org/10.1016/j.ijpharm.2013.06.016

Foroozandeh, P., & Aziz, A. A. (2018). Insight into cellular uptake and intracellular trafficking of nanoparticles. *Nanoscale Research Letters, 13*, 339. https://doi.org/10.1186/s11671-018-2728-6

Fu, Z., Ju, H., Xu, G. S., Wu, Y. C., Chen, X., & Li, H. J. (2024). Recent development of carrier materials in anthocyanins encapsulation applications: A comprehensive literature review. *Food Chemistry, 439*. https://doi.org/10.1016/j.foodchem.2023.138104

Ghareaghajlou, N., Hallaj-Nezhadi, S., & Ghasempour, Z. (2021). Red cabbage anthocyanins: Stability, extraction, biological activities and applications in food systems. *Food Chemistry, 365*. https://doi.org/10.1016/j.foodchem.2021.130482

Gou, J., Feng, S., Liang, Y., Fang, G., Zhang, H., Yin, T., & Tang, X. (2017). Polyester–Solid Lipid Mixed Nanoparticles with Improved Stability in Gastro-Intestinal Tract Facilitated Oral Delivery of Larotaxel. *Molecular Pharmaceutics, 14*(11), 3750–3761. https://doi.org/10.1021/acs.molpharmaceut.7b00503

Hadji, H., & Bouchemal, K. (2022). Effect of micro- and nanoparticle shape on biological processes. *Journal of Controlled Release, 342*, 93–110. https://doi.org/10.1016/j.jconrel.2021.12.032

Hillaireau, H., & Couvreur, P. (2009). Nanocarriers' entry into the cell: Relevance to drug delivery. *Cellular and Molecular Life Sciences, 66*(17), 2873–2896. https://doi.org/10.1007/s00018-009-0053-z

Hsein, H., Garrait, G., Beyssac, E., & Hoffart, V. (2015). Whey protein mucoadhesive properties for oral drug delivery: Mucin–whey protein interaction and mucoadhesive bond strength. *Colloids and Surfaces B: Biointerfaces, 136*, 799–808. https://doi.org/10.1016/j.colsurfb.2015.10.016

Huang, J. G., Leshuk, T., & Gu, F. X. (2011). Emerging nanomaterials for targeting subcellular organelles. *Nano Today, 6*(5), 478–492. https://doi.org/10.1016/j.nantod.2011.08.002

Jiang, P., Huang, J., Bao, C., Jiao, L. L., Zhao, H. Y., Du, Y. Z., & Li, Y. (2018). Enzymatically partially hydrolyzed alpha-Lactalbumin peptides for self-assembled micelle formation and their application for Coencapsulation of multiple antioxidants. *Journal of Agricultural and Food Chemistry, 66*(49), 12921–12930. https://doi.org/10.1021/acs.jafc.8b03798

Koh, Y.-C., Tsai, Y.-W., Lee, P.-S., Nagabhushanam, K., Ho, C.-T., & Pan, M.-H. (2022). Amination potentially augments the ameliorative effect of curcumin on inhibition of the IL-6/Stat3/c-Myc pathway and gut microbial modulation in colitis-associated tumorigenesis. *Journal of Agricultural and Food Chemistry, 70*(46), 14744–14754. https://doi.org/10.1021/acs.jafc.2c06645

Li, D., Liu, A., Liu, M., Li, X., Guo, H., Zuo, C., & Li, Y. (2020). The intestine-responsive lysozyme nanoparticles-in-oxidized starch microgels with mucoadhesive and penetrating properties for improved epithelium absorption of quercetin. *Food Hydrocolloids, 99*, Article 105309. https://doi.org/10.1016/j.foodhyd.2019.105309

Li, L. P., He, S. J., Yu, L. Z., Elshazly, E. H., Wang, H., Chen, K. M., & Gong, R. M. (2019). Codelivery of DOX and siRNA by folate-biotin-quaternized starch nanoparticles for promoting synergistic suppression of human lung cancer cells. *Drug Delivery, 26*(1), 499–508. https://doi.org/10.1080/10717544.2019.1606363

Li, X., Jafari, S. M., Zhou, F., Hong, H., Jia, X., Mei, X., & Li, Y. (2023). The intracellular fate and transport mechanism of shape, size and rigidity varied nanocarriers for understanding their oral delivery efficiency. *Biomaterials, 294*, Article 121995. https://doi.org/10.1016/j.biomaterials.2023.121995

Li, Y., de Vries, R., Slaghek, T., Timmermans, J., Cohen Stuart, M. A., & Norde, W. (2009). Preparation and characterization of oxidized starch polymer microgels for encapsulation and controlled release of functional ingredients. *Biomacromolecules, 10*(7), 1931–1938. https://doi.org/10.1021/bm900337n

Li, Y., Yang, Y. H., Zhu, S., Liu, B., Zhong, F., & Huang, D. J. (2023). Tea polyphenols-OSA starch interaction and its impact on interface properties and oxidative stability of O/W emulsion. *Food Hydrocolloids, 135*, Article 108187. https://doi.org/10.1016/j.foodhyd.2022.108187

Ling, K., Wu, H. X., Neish, A. S., & Champion, J. A. (2019). Alginate/chitosan microparticles for gastric passage and intestinal release of therapeutic protein nanoparticles. *Journal of Controlled Release, 295*, 174–186. https://doi.org/10.1016/j.jconrel.2018.12.017

Marze, S. (2022). Compositional, Structural, and Kinetic Aspects of Lipid Digestion and Bioavailability: In Vitro, In Vivo, and Modeling Approaches. *Annual Review of Food Science and Technology, 13*, 263–286. https://doi.org/10.1146/annurev-food-052720-093515

Neves, A. R., Martins, S., Segundo, M. A., & Reis, S. (2016). Nanoscale delivery of resveratrol towards enhancement of supplements and nutraceuticals. *Nutrients, 8*(3), 131. https://www.mdpi.com/2072-6643/8/3/131.

Neves, A. R., Queiroz, J. F., Costa Lima, S. A., Figueiredo, F., Fernandes, R., & Reis, S. (2016). Cellular uptake and transcytosis of lipid-based nanoparticles across the intestinal barrier: Relevance for oral drug delivery. *Journal of Colloid and Interface Science, 463*, 258–265. https://doi.org/10.1016/j.jcis.2015.10.057

das Neves, J., Arzi, R. S., & Sosnik, A. (2020). Molecular and cellular cues governing nanomaterial-mucosae interactions: From nanomedicine to nanotoxicology. *Chemical Society Reviews, 49*(14), 5058–5100. https://doi.org/10.1039/c8cs00948a

Ozel, B., Zhang, Z. Y., He, L. L., & McClements, D. J. (2020). Digestion of animal- and plant-based proteins encapsulated in kappa-carrageenan/protein beads under simulated gastrointestinal conditions. *Food Research International, 137*, Article 109662. https://doi.org/10.1016/j.foodres.2020.109662

Qiu, Y., Liu, Y., Wang, L. M., Xu, L. G., Bai, R., Ji, Y. L., & Chen, C. Y. (2010). Surface chemistry and aspect ratio mediated cellular uptake of au nanorods. *Biomaterials, 31*(30), 7606–7619. https://doi.org/10.1016/j.biomaterials.2010.06.051

Rydberg, H. A., Arteta, M. Y., Berg, S., Lindfors, L., & Sigfridsson, K. (2016). Probing adsorption of DSPE-PEG2000 and DSPE-PEG5000 to the surface of felodipine and griseofulvin nanocrystals. *International Journal of Pharmaceutics, 510*(1), 232–239. https://doi.org/10.1016/j.ijpharm.2016.06.046

Sahay, G., Alakhova, D. Y., & Kabanov, A. V. (2010). Endocytosis of nanomedicines. *Journal of Controlled Release, 145*(3), 182–195. https://doi.org/10.1016/j.jconrel.2010.01.036

Sannidhi, A., Zhou, C., Choi, Y. S., David, A. E., Todd, P. W., & Hanley, T. R. (2023). Nanomaterial endocytosis: Quantification of adsorption and ingestion mechanisms. *Magnetochemistry, 9*(2), 37. https://www.mdpi.com/2312-7481/9/2/37.

Serra, L., Domenech, J., & Peppas, N. A. (2009). Engineering design and molecular dynamics of mucoadhesive drug delivery systems as targeting agents. *European Journal of Pharmaceutics and Biopharmaceutics, 71*(3), 519–528. https://doi.org/10.1016/j.ejpb.2008.09.022

Shen, X., Zhao, C., Lu, J., & Guo, M. (2018). Physicochemical properties of whey-protein-stabilized Astaxanthin Nanodispersion and its transport via a Caco-2 monolayer. *Journal of Agricultural and Food Chemistry, 66*(6), 1472–1478. https://doi.org/10.1021/acs.jafc.7b05284

Shen, Y., Zhang, N., Tian, J., Xin, G., Liu, L., Sun, X., & Li, B. (2022). Advanced approaches for improving bioavailability and controlled release of anthocyanins. *Journal of Controlled Release, 341*, 285–299. https://doi.org/10.1016/j.jconrel.2021.11.031

Subramanian, D. A., Langer, R., & Traverso, G. (2022). Mucus interaction to improve gastrointestinal retention and pharmacokinetics of orally administered nano-drug delivery systems. *Journal of Nanobiotechnology, 20*(1), 362. https://doi.org/10.1186/s12951-022-01539-x

Talegaonkar, S., & Bhattacharyya, A. (2019). Potential of Lipid Nanoparticles (SLNs and NLCs) in Enhancing Oral Bioavailability of Drugs with Poor Intestinal Permeability. *AAPS Pharm Sci Tech, 20*(3), 121. https://doi.org/10.1208/s12249-019-1337-8

Tan, X. Y., Yin, N., Liu, Z. X., Sun, R., Gou, J. X., Yin, T., & Tang, X. (2020). Hydrophilic and electroneutral nanoparticles to overcome mucus trapping and enhance Oral delivery of insulin. *Molecular Pharmaceutics, 17*(9), 3177–3191. https://doi.org/10.1021/acs.molpharmaceut.0c00223

Teo, A., Lee, S. J., Goh, K. K. T., & Wolber, F. M. (2017). Kinetic stability and cellular uptake of lutein in WPI-stabilised nanoemulsions and emulsions prepared by emulsification and solvent evaporation method. *Food Chemistry, 221*, 1269–1276. https://doi.org/10.1016/j.foodchem.2016.11.030

Tong, Y. Q., Li, L., & Meng, X. J. (2023). Anthocyanins from Aronia melanocarpa bound to amylopectin nanoparticles: Tissue distribution and in vivo oxidative damage protection. *Journal of Agricultural and Food Chemistry, 71*(1), 430–442. https://doi.org/10.1021/acs.jafc.2c06115

Ubaidulla, U., Priyanka, S., Sangavi, T., & Grace, R. (2022). Development of silymarin entrapped chitosan phthalate nanoparticles for targeting colon cancer. *Journal of Natural Remedies, 22*(4), 659–671. https://doi.org/10.18311/jnr/2022/29816

Wang, S. S., Chen, Y. Y., Lang, H., Chen, Y. M., Shi, M. X., Wu, J. D., & Li, Y. (2015). Intestine-specific delivery of hydrophobic bioactives from oxidized starch microspheres with an enhanced stability. *Journal of Agricultural and Food Chemistry, 63*(39), 8669–8675. https://doi.org/10.1021/acs.jafc.5b03575

Wang, W., Liu, Q. Y., Liang, X. C., Kang, Q., & Wang, Z. N. (2022). Protective role of naringin loaded solid nanoparticles against aflatoxin B1 induced hepatocellular carcinoma. *Chemico-Biological Interactions, 351*, Article 109711. https://doi.org/10.1016/j.cbi.2021.109711

Wang, W., Liu, W., Wu, J., Liu, M., Wang, Y., Liu, H., & Liu, J. (2024). Preparation and characterization of particle-filled microgels by chemical cross-linking based on zein and carboxymethyl starch for delivering the quercetin. *Carbohydrate Polymers, 323*, Article 121375. https://doi.org/10.1016/j.carbpol.2023.121375

Wang, Z. R., Li, Y., Chen, L., Xin, X. L., & Yuan, Q. P. (2013). A study of controlled uptake and release of anthocyanins by oxidized starch microgels. *Journal of Agricultural and Food Chemistry, 61*(24), 5880–5887. https://doi.org/10.1021/jf400275m

Wu, H. Y., Zhang, H. Y., Li, X. H., Secundo, F., & Mao, X. Z. (2023). Preparation and characterization of phosphatidyl-agar oligosaccharide liposomes for astaxanthin encapsulation. *Food Chemistry, 404*, Article 134601. https://doi.org/10.1016/j.foodchem.2022.134601

Wu, J., Shi, M., Li, W., Zhao, L., Wang, Z., Yan, X., & Li, Y. (2015). Pickering emulsions stabilized by whey protein nanoparticles prepared by thermal cross-linking. *Colloids and Surfaces. B, Biointerfaces, 127*, 96–104. https://doi.org/10.1016/j.colsurfb.2015.01.029

Xiong, K., Zhou, L. Y., Wang, J. Y., Ma, A. G., Fang, D., Xiong, L., & Sun, Q. J. (2020). Construction of food-grade pH-sensitive nanoparticles for delivering functional food ingredients. *Trends in Food Science & Technology, 96*, 102–113. https://doi.org/10.1016/j.tifs.2019.12.019

Yuan, Y., Liu, Y., He, Y., Zhang, B. K., Zhao, L., Tian, S. M., & Li, Y. (2022). Intestinal-targeted nanotubes-in-microgels composite carriers for capsaicin delivery and their effect for alleviation of Salmonella induced enteritis. *Biomaterials, 287*, Article 121613. https://doi.org/10.1016/j.biomaterials.2022.121613

Zhang, Y. J., Abidi, W., & Berlin, J. M. (2019). Colloidal capsules assembled from gold nanoparticles using small-molecule hydrophobic cross-linkers. *Langmuir, 35*(52), 17037–17045. https://doi.org/10.1021/acs.langmuir.9b01903

Zhu, C. L., Huo, D., Chen, Q. S., Xue, J. J., Shen, S., & Xia, Y. N. (2017). A eutectic mixture of natural fatty acids can serve as the gating material for near-infrared-triggered drug release. *Advanced Materials, 29*(40), 1703702. https://doi.org/10.1002/adma.201703702